Journal of
Mechanics of
Materials and Structures

NUMERICAL AND EXPERIMENTAL ANALYSIS OF THE STATIC COMPLIANCE OF CHIRAL TRUSS-CORE AIRFOILS

Alessandro Spadoni and Massimo Ruzzene

Volume 2, Nº 5 May 2007

mathematical sciences publishers

JOURNAL OF MECHANICS OF MATERIALS AND STRUCTURES
Vol. 2, No. 5, 2007

NUMERICAL AND EXPERIMENTAL ANALYSIS OF THE STATIC COMPLIANCE OF CHIRAL TRUSS-CORE AIRFOILS

ALESSANDRO SPADONI AND MASSIMO RUZZENE

This paper presents an innovative wing profile featuring an internal truss-like structure of chiral topology. The chiral design is selected because of its unique deformation characteristics, which produce a theoretical, in-plane Poisson's ratio of -1. Such a Poisson's ratio yields a very high shear modulus, which in principle does not require the wing profile to be defined by a closed section or stressed-skin configuration. In addition, the peculiar deformation mechanism of the chiral configuration allows large decambering deflections to occur, with all the members of assembly behaving within the linear range of the material. Hence the proposed design combines large chordwise compliance and large in-plane shear stiffness. Such conflicting mechanical properties can be achieved through the proper selection of a limited number of geometric parameters defining the core configuration. The objective of the paper is to investigate the compliance characteristics of the airfoil. Two-dimensional profiles, designed according to results from previous investigations, are manufactured and tested to assess compliance and evaluate decambering deflection limits. The experimental analysis is guided by numerical models that account for deviations from the ideal configuration due to manufacturing limitations. Numerical and experimental results demonstrate the influence of core geometry on the compliance and confirm the ability of chiral-core airfoils to sustain large deflections while not exceeding yield strain limits.

1. Introduction

Since the first attempts of powered flight, researchers have tried to devise techniques to implement morphing as a form of flight control. Most notably, the Wright brothers utilized controlled warping of the wings of Wright Flyer to achieve lateral control [Culik 2003]. More recently, the introduction of smart structures and adaptive technologies in the aerospace field has offered opportunities to implement novel structural morphing concepts [McGowan et al. 2003]. In general, morphing requires structural compliance which often conflicts with stiffness requirements for carrying prescribed aerodynamic loads. Among the various configurations investigated, the *belt rib concept* [Campanile and Sachau 2000] allows the achievement of continuous camber variations by transferring the stroke of an actuator to a geometric shape change of the airfoil through a closed belt and an internal structural network. A similar, remarkable solution for camber variation is the *finger concept* [Monner et al. 2000], where the airfoil features a flexible rib composed of plate-like elements connected through revolute joints. Tension-torsion coupling has been employed as an effective means to actively control camber in helicopter blades [Büter et al. 2001], while other design solutions have considered inflatable airfoil structures [Cadogan et al. 2004],

Keywords: morphing airfoils, aeroelastic tailoring, chiral topology, truss-core airfoils.
The authors wish to thank the Army Research Office (ARO) for the support provided for this work under the grant 45518-EG.

variable-span morphing wings [Trenker 2003; Bae et al. 2004], and hingeless flexible leading and trailing edges actuated using shape memory alloys [Kudva 2004].

Cellular materials are applied for the design of structural components with superior mechanical properties and multifunctional characteristics. Their properties are topology dependent, that is, they are a function of the geometry and of the shape of the elementary cell composing the assembly. Cell shape and geometry can be tailored to satisfy requirements of a given application or to achieve various functionalities. The chiral geometry, introduced in [Lakes 1991] and studied extensively in [Prall and Lakes 1997], is a configuration whose negative in-plane Poisson's ratio leads to a very high shear modulus, while featuring some degree of in-plane bending compliance. From a continuum point of view, a structural component defined by periodic structure whose unit cell is the chiral honeycomb may be able to carry higher torsional and shear loads, if compared to the same component made of solid material such as aluminum, which usually possesses a Poisson's ratio of 0.33. This unusual mechanical behavior can be exploited for the design of sandwich structures with chiral truss core as presented in [Spadoni and Ruzzene 2006; Spadoni et al. 2006]. The chiral structure can be accommodated within an airfoil, so that its compliant characteristics can be used to achieve chordwise bending. The deformation mechanisms of chiral structures allow continuous deformations of the airfoil to occur with all the individual members undergoing strains within the linear range of the material. The ability to sustain large deformations without exceeding yield conditions is required to achieve repeatability, while smooth deformations are required for aerodynamic efficiency.

The objective of this paper is to investigate the compliance of the proposed configuration. The work continues previous investigations presented in [Spadoni and Ruzzene 2006], where a coupled-physics model, comprised of weakly-coupled CFD and linear, elastostatic structural analyses, was developed to investigate the influence of the core configuration on the static aeroelastic behavior of the airfoil. Results in [Spadoni and Ruzzene 2006] showed that significant changes in the bending compliance can be achieved through the variation of the geometric parameters defining the core layout. The results of [Spadoni and Ruzzene 2006] are used to select three airfoil designs to be manufactured and tested. The experiments are guided by a numerical analysis performed using nonlinear FE models, which account for deviations in geometry from the ideal configuration introduced by the manufacturing process.

The paper is organized as follows. This introduction is followed by a section describing the motivation for this work, the concept under investigation and the main parameters considered in the analysis. Section 3 presents the airfoil design process and the numerical investigations performed to extend the work in [Spadoni and Ruzzene 2006]. Section 4 describes experimental set-up, procedures and results, and finally Section 5 summarizes the work and provides recommendation for future investigations.

2. Motivations and objectives

2.1. ***Overview.*** The design of deformable systems may be driven by kinematic or mechanical considerations, according to the manner in which the system's deformations take place. Deformations may be desired to alleviate structural stresses, they may be passive in nature and arise from low structural stiffness, or they may be actively induced, as in the case of structural mechanisms. Often, the ability of a structural system to deform is coupled with strength requirements, which often arise in applications for which weight considerations drive the design. Aircraft are a prime example of such requirements. Given

the state-of-the-art, it is common practice to select an aircraft configuration based on the most frequent conditions encountered during a mission. For a passenger aircraft, for example, cruise conditions dictate the design. The lifting surfaces may be optimized to maximize the lift-to-drag ratio (L/D) at cruise conditions, but they also need to operate properly even for off-design conditions. Such requirements are satisfied by wing reconfiguration, which is often justified in terms of efficiency, while it is in fact required to sustain flight. The deformations to which lifting surfaces are subjected can be divided into passive, due to aeroelastic phenomena, and active, due to the actuation of mechanisms for reconfiguration such as flaps and slats. Elastic deformations may be further differentiated into span-wise and chord-wise directions. Span-wise deformations may be of torsional, bending or shearing nature. Spanwise bending is usually sought to relieve wing-root stresses, while spanwise torsion is to be avoided as it is one of the major causes of aeroelastic divergence, aileron reversal, and flutter [Hodges and Pierce 2002]. Chordwise deformations are currently avoided as they alter wing section aerodynamic characteristics, and, more importantly, the spanwise characteristics of a wing [Ghiringhelli and Mantegazza 1994; Hodges and Pierce 2002], while highly coupling the design of reconfiguration mechanisms with elastic phenomena. However, exploiting elastic deformations for control and aeroelastic tailoring purposes could yield enormous reductions in complexity and weight.

2.2. ***Geometry of chiral layout.*** The proposed wing design exploits the mechanical characteristics of the chiral topology shown in Figure 1 [Lakes 1991; Prall and Lakes 1997]. The layout consists of circular elements acting as nodes, connected by ribs or ligaments tangent to the nodes. The parameters defining the geometry are R, L, β, t, and θ, which in turn define the distance between the node centers, the rib length, the angle between the imaginary line connecting circles centers and a rib, the wall thickness, and the angle defining unit cell's width to height ratio. The following relations hold [Prall and Lakes 1997]:

$$\tan(\beta) = \frac{2r}{L} \tag{1}$$

$$\sin(\beta) = \frac{2r}{R} \tag{2}$$

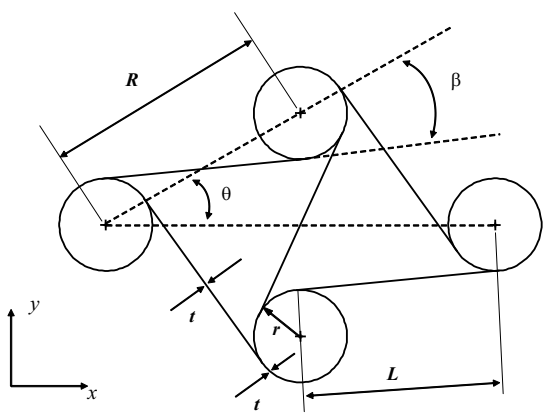

Figure 1. Chiral configuration and parameters defining the unit configuration.

$$\sin(\theta) = \frac{R}{R/2} \tag{3}$$

The resulting cellular structure is characterized by a nonclassical mechanical behavior due to its negative in-plane Poisson's ratio theoretically ≈ -1 [Prall and Lakes 1997], in addition to the ability to undergo large displacements while operating in the elastic range of the constituent material [Prall and Lakes 1997]. Such unusual Poisson's ratio leads to unique deformation characteristics [Prall and Lakes 1997], which include rotational degrees of freedom (DOF) in addition to translational DOF's, and in principle provides the assembly with a very high in-plane shear modulus. A negative Poisson's ratio also affects the dynamics response of assemblies [Lakes 1991]. Moreover, its properties can be altered through variations of geometric parameters such as the ratio of rib length L to node radius R. Examples of configurations with different L/R ratios are shown in Figure 2.

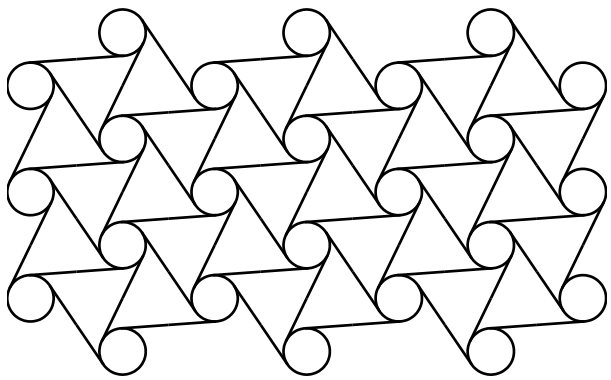

(a) $L/R = 0.90$

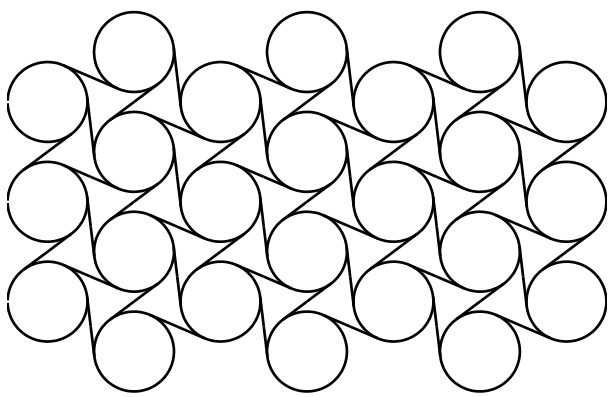

(b) $L/R = 0.60$

Figure 2. Variation of chiral lattice characteristics with L/R ratio.

2.3. ***Objectives and relation to previous investigations.*** Initial investigations on the application of the chiral geometry to morphing can be found in [Bornengo et al. 2005], where the performance of a conformable race car wing is analyzed through a numerical model. In [Bornengo et al. 2005], the airfoil core is modeled as a homogeneous material with the mechanical properties of a homogenized chiral assembly. This implicitly assumes that the unit cell size is much smaller than the dimensions of the wing. Subsequent studies [Spadoni and Ruzzene 2006; Spadoni et al. 2006] have instead considered configurations where the cell has dimensions of the order of those of the structure (Figure 3). Both in [Bornengo et al. 2005] and in [Spadoni and Ruzzene 2006], an Eppler 420 profile is considered. Such a highly cambered airfoil is chosen to demonstrate the compliance of the assembly, as the deformations that are sought involve decambering effects. In [Spadoni and Ruzzene 2006] the compliance of the core airfoil, in terms of de-cambering deformations due to aerodynamic loads, was investigated through weakly coupled CFD and linear, elastostatic FE models. The results showed the strong influence of the core configuration, and specifically how number of cells and L/R ratio can be selected to achieve desired levels of de-cambering deformations for assigned flow conditions.

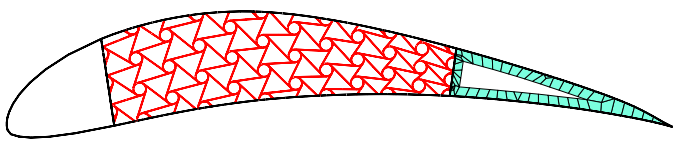

Figure 3. Truss-core airfoil configuration.

The main objective of the current paper is to investigate the properties of the chiral core airfoil experimentally. While in [Spadoni and Ruzzene 2006], the loads applied to the FE models were distributed pressures of aerodynamic nature, the experimental tests on the manufactured airfoil samples involve a simplified scenario whereby mechanical point-loads are employed to promote bending. Specifically, the de-cambering deformations of the airfoil as a result of increasing mechanical loads are measured while monitoring the strain at selected locations. The purpose of the tests is to verify the strong influence of core design on airfoil compliance and to estimate maximum deflections achievable in the elastic range of the material. The tests are guided by a numerical model, which is used to predict load values to be considered in the experiments. The model is significantly different from the one used in previous investigations [Spadoni and Ruzzene 2006]. First, material nonlinearities are introduced to enable the prediction of loads causing the material to enter the plastic range. In addition, the geometry of the structure is modified to reflect variations from the ideal geometry due to the water jet manufacturing process employed for the fabrication of the samples. In particular, a perfect tangency condition between nodes and ligaments cannot be reproduced. Fillets between nodes and ligaments are included in the FE model in an attempt to reproduce the geometry of the test specimens. The presence of fillets is important as it may in fact modify the bending behavior of the ligaments, which is the leading mechanism of deformation of the chiral structure [Lakes 1991].

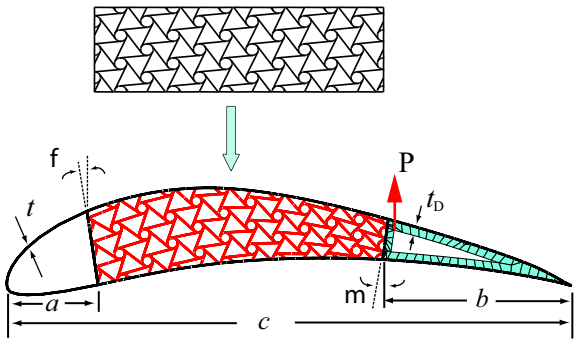

Figure 4. Mapped chiral-core configuration.

3. Design, manufacturing and modeling

3.1. ***Airfoil configurations.*** The configuration of the core is defined by selecting a periodic, two-dimensional chiral lattice with specified number of cells and L/R ratio. The resulting geometry is then mapped into the airfoil profile (Eppler 420) through a simple coordinate transformation. The procedure is depicted schematically in Figure 4. The configurations considered for the analysis are depicted in Figure 5. Such geometries, selected on the basis of results from [Spadoni and Ruzzene 2006], are respectively defined by 2 cells across the thickness and $L/R = 0.60$ (Figure 5a), 3 cells across the thickness and $L/R = 0.60$ (Figure 5b), and 3 cells across the thickness and $L/R = 0.94$ (Figure 5c). In the remainder of the paper, the airfoil of Figure 5a will be referred to as configuration a, the one depicted in Figure 5b will

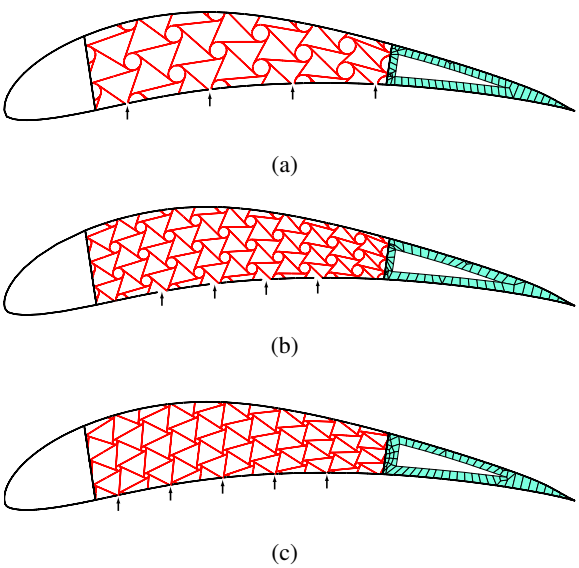

Figure 5. Mapped chiral-core configurations.

be referred to as configuration b, and the one depicted in Figure 5c will be denoted as configuration c. The following wing dimensions are selected on the basis of manufacturing constraints: chord $c = 0.7$ m, angle $\phi = 8.58°$, angle $\mu = 8.0°$, lengths a and b respectively equal to 11 and 23.5 cm, and wall nominal thickness of core structure and skins $t = 0.76$ mm. The out-of-plane thickness of the structure is 1.9 cm. The shaded area in the trailing-edge region (Figure 4) is obtained by offsetting the trailing-edge profile by 2.54 cm. The resulting thickness on the upper and lower trailing-edge boundaries, t_D is then 2.54 cm.

In an attempt to maximize deflections, the lower skin of each airfoil configuration has been cut at the locations indicated by arrows in Figure 5. In the proposed design, the skin has been found to act as an obstacle to the decambering deformation. The ability to carry shear loads illustrated in [Spadoni and Ruzzene 2006] and the potential torsional rigidity of the chiral design due to its negative Poisson's ratio suggest that the classic closed section with stressed skin may not be necessary. In fact the core itself may provide sufficient torsional and shear-loads carrying capacity, that the skins would only be used to provide the surface continuity dictated by aerodynamic requirements. Additional developments of the concept would therefore require the investigation of the application of flexible skins, able to conform to the airfoil, to allow de-cambering deflections, while maintaining smoothness of the airfoil surface. For simplicity of manufacturing, the airfoil is cut out of a solid aluminum plate so that the entire assembly is made of a single material. This leads to skins that are unnecessarily stiff. The decision to cut them at selected locations is simply motivated by the need to reduce the complexity of manufacturing and to avoid the issue of the skin design, which is currently under investigation. Finally, although the proposed design may present complexities that currently outweigh the choice of conventional wing assemblies over their truss-core counterparts, the aim is to demonstrate a concept of a multifunctional and adaptable wing which does not require control surfaces, and may offer optimal aerodynamic characteristics on a wide range of flight regimes.

3.2. ***Manufacturing.*** Three truss-core airfoils matching the configurations of Figure 5 have been manufactured using an OMAX® water-jet cutting machine out of a plate of aluminum 1.9 cm thick. The resulting test specimens are shown in Figure 6. Manufacturing constraints imposed the presence of fillets at the locations where ligaments join with nodes. The radius of such fillets was estimated to be of the order of 0.13 mm. In addition, the thickness of the ligaments, nominally designed to be 0.76 mm, was found upon measurement to vary between 0.66 and 0.80 mm.

3.3. ***Numerical model.*** A structural FE model is developed to investigate the ability of the airfoil to undergo large chord-wise deformations while within the linear range of the material. The model includes material nonlinearity to allow the estimation of load limits for the onset of plastic deformations. Such limits are used as guidelines during the experiments. In the model, developed using the commercially available software ANSYS®, the material behavior is described by a bilinear stress-strain relation, which approximates the behavior of the selected material (Aluminum 6061 $T651$: Young's modulus $E = 69$ GPa, density $\rho = 2700\,\mathrm{Kg/m^3}$, Poisson's ratio $\nu = 0.33$, yield stress $\sigma_y = 276$ MPa, and tangent modulus $E_t = 100$ MPa) [Herbert et al. 2006]. In the model, the leading edge region is considered completely clamped and therefore it is not modeled. The trailing-edge regions are made of solid material, while the remaining portions of the wing feature beam-like components. The resulting two-dimensional FE model includes bilinear, 4-node, plane elements and beam elements with both axial and transverse degrees of freedom. The plane element used is PLANE42 [ANSYS 2005], which features 4 nodes and 2 DOF per

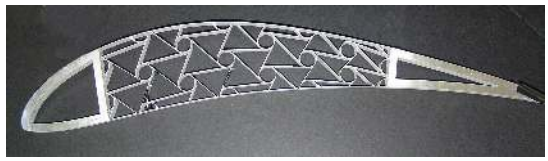

(a)

(b)

(c)

Figure 6. Manufactured truss-core airfoils.

node to describe the in-plane displacements. The beam element (BEAM23 [ANSYS 2005]), features axial and transverse DOF's to describe axial, bending and shear deformations. Both BEAM23 and PLANE42 elements have plastic deformation capabilities. In addition, PLANE42 elements are added in the filleted regions shown in Figure 7. The ligaments discretization is also refined in an attempt to better capture stress concentrations expected at the aforementioned locations. Finally, the presence of

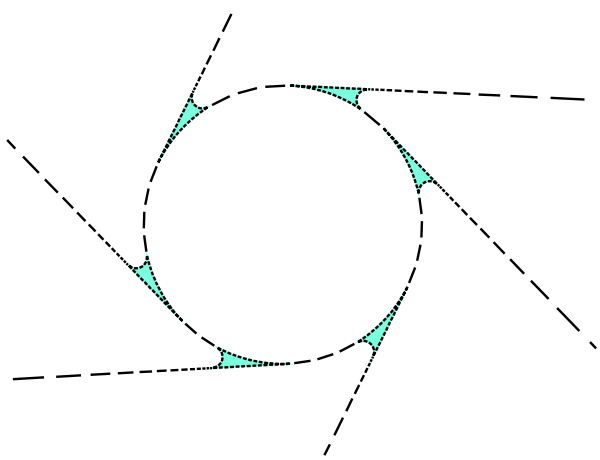

Figure 7. Detail of core discretization with fillets at the nodes/ligaments joints.

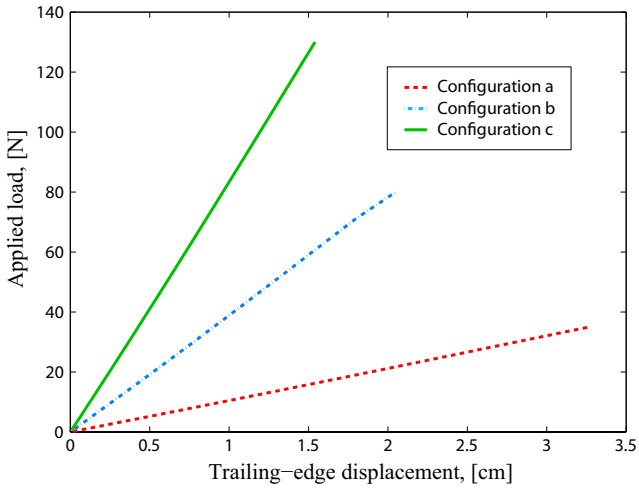

Figure 8. Load, trailing-edge displacement relationship for the considered configurations.

thickness irregularities in the test samples is reproduced by randomly assigning the wall thickness t of each beam element in the interval $[0.66, 0.80]$ mm.

4. Results

4.1. *Numerical results.*

4.2. ***Experimental set-up.*** The deflections of the wing profile are induced by a concentrated mechanical load applied at the location shown in Figure 4. This loading configuration reproduces the one considered experimentally as described in Section 3. The numerical model is used to evaluate the compliance of the three considered configurations, and to identify load ranges to be used during the experiments. Load/displacement curves for the three configurations are plotted in Figure 8, which shows, in adherence with the results of [Spadoni and Ruzzene 2006], that configuration a is the most compliant, while configuration c is the least compliant. The maximum load applied to each airfoil is selected in order to obtain clear onset of plastic deformations in parts of the structure: for configuration a, the maximum load is 35 N, for configuration b is 80 N, while for configuration c is 130 N. Figure 9 shows the von Mises stress distribution immediately before the onset of plastic deformations. In all cases, the highest stresses appear within the core, and in particular, where ligaments join nodes. It is interesting to note that the locations of highest stress are different for each configuration. Such disparities may be attributed to the different deformation mechanisms that arise by varying the geometry of the honeycomb core by modifying the ratio L/R. The maximum von Mises stress within the considered assemblies follows the stress-strain curve of the constitutive material, as shown in Figure 10.

The experimental setup is depicted in Figure 11. It consists of a Linear Variable Displacement Transducer (LVDT) from RDP® (Model DCTH) and associated power supply (Agilent®, Model E3641A), to measure the trailing edge deflection. The strain in selected structural members is measured by a set of strain gages (VISHAY® CEA-13-125UN-120). The strain gages are applied to the ligaments within the

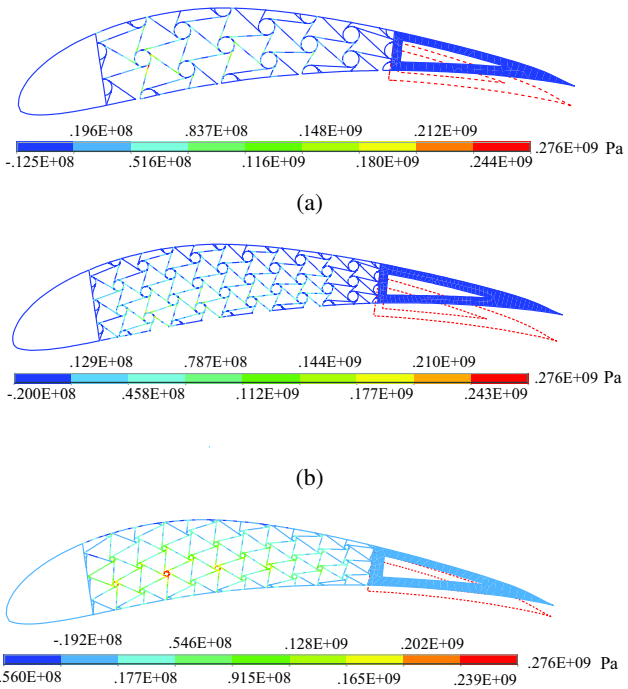

Figure 9. Von Mises stress distribution of considered configurations.

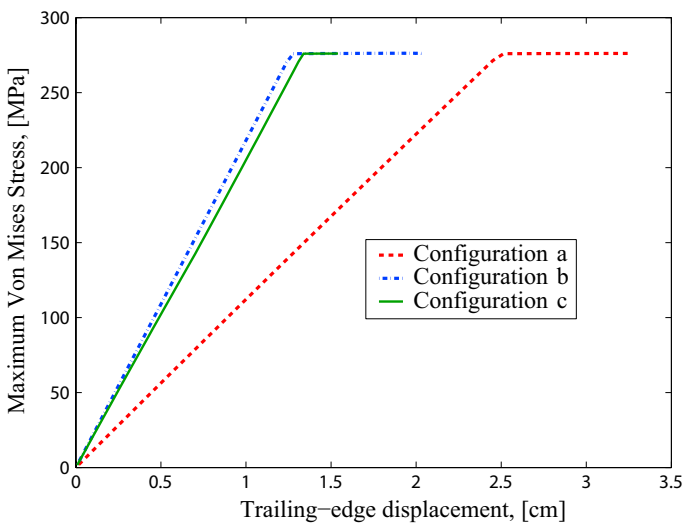

Figure 10. Maximum von Mises stress, trailing-edge displacement relationship for the considered configurations.

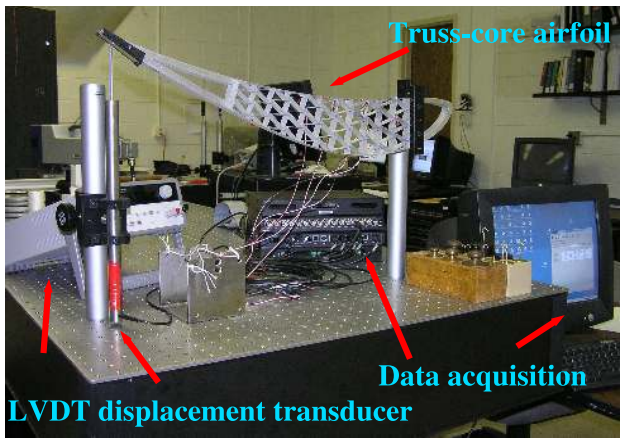

Figure 11. Experimental setup.

truss core and on the airfoil profile based on the stress distribution observed from numerical simulations. The selected locations for the strain gages are depicted in Figure 12, which also shows point of load application and location of the LVDT. The stress distribution within a ligament can be estimated from the linear-elastic deformation mechanism proposed by [Prall and Lakes 1997] and depicted in Figure 13.

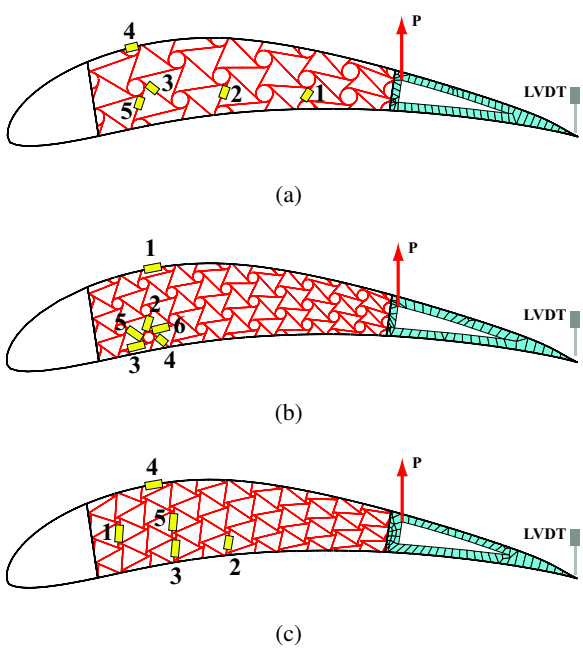

Figure 12. Strain gage, load and LVDT locations.

Loading of the chiral lattice causes rotation of the nodes and bending of the ligaments as depicted in Figure 13. Neglecting shear deformations, the resulting axial strain distribution within a ligament varies linearly along the length from a negative to a positive value, so that, at mid span, the axial strain is approximately 0. The highest axial strain is then expected at the location where ligaments join nodes in a tangential fashion. Consequently, the strain gages are placed on the ligaments, as close to the nodes as possible.

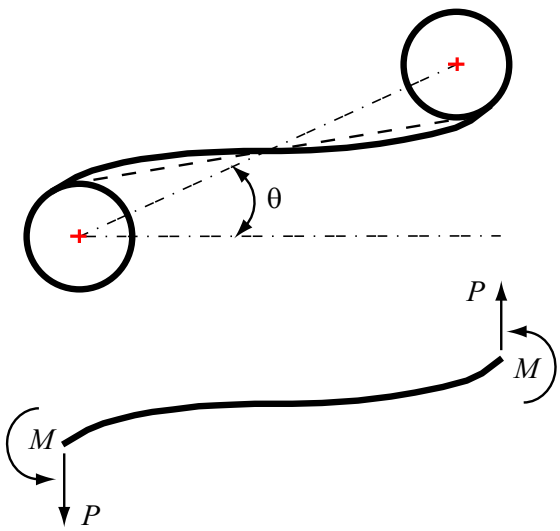

Figure 13. Deformation mechanism proposed by [Prall and Lakes 1997].

4.3. ***Results and comparison with numerical predictions.*** The truss-core airfoils depicted in Figure 6 are loaded as described in the previous section. In the experiments, each specimen is subjected to a loading/unloading cycle to observe deviations from linearity, hysteresis and the presence of residual deformations upon unloading. To preserve the integrity of the manufactured samples for future tests, the maximum applied load is maintained below the value which numerical results indicate capable of producing plastic deformations. The numerical analysis in certain circumstances, however, lacks the ability to accurately predict stress concentrations, even with very refined meshes. This is certainly the case for the models presented in the current work, where thin, beam-like members are connected to much more rigid nodes. The load/trailing edge displacement variation for configuration *a* is shown in Figure 14, which directly compares experimental measurements and numerical predictions. The plot shows good agreement and indicates the presence of some hysteresis. Such hysteresis can be associated to friction at the airfoil/LVDT contact region, and internal to the LVDT itself. In addition, a residual displacement is observed upon unloading. The strain recorded at location 5 (see Figure 12) shown in Figure 15 also indicates the presence of a residual strain upon unloading. Figure 15 presents for completeness the strain predicted at location 4, whose variation highlights a discrepancy between numerical and experimental strain. Such a discrepancy may be attributed to the fact that strain gages may not have been placed

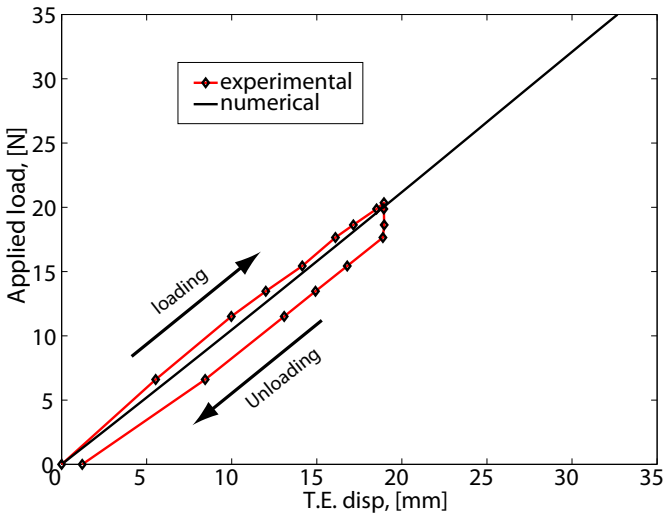

Figure 14. Numerical and experimental trailing-edge displacement for configuration a.

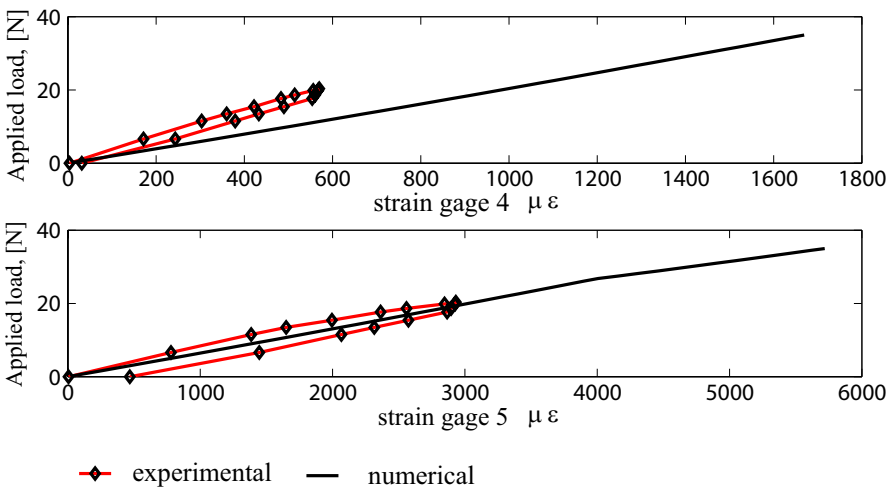

Figure 15. Numerical and experimental strain for configuration a.

exactly on the location of maximum strain, and that the strain is averaged over the gage area, while a point, nodal value is extracted from the FE results.

The results for configuration b presented in Figure 17 show an excellent agreement between measurements and numerical predictions. As opposed to the previous case, no residual displacement is observed, indicating that, for configuration b, all trailing edge displacement is recovered upon unloading. The absence of plastic deformations in the material is confirmed by the strain variation at location 5 (see Figure 12) shown in Figure 16. The strain variation at another location (location 2) does not show the same level of agreement, but confirms the absence of residual strains. It should be observed that the

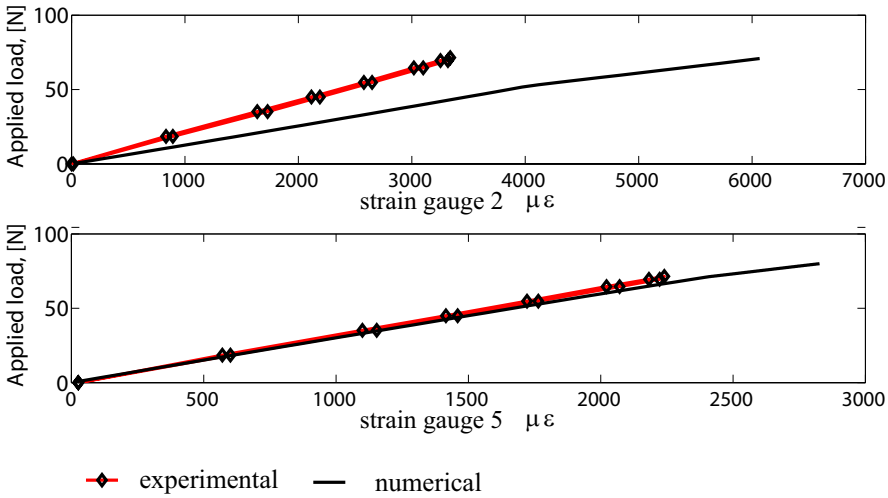

Figure 16. Numerical and experimental strain for configuration *b*.

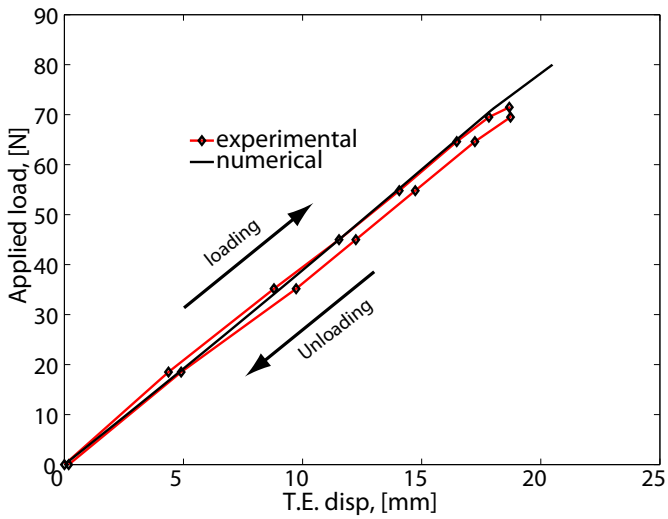

Figure 17. Numerical and experimental trailing-edge displacement for configuration *b*.

application of strain gages on configuration *b* was made more difficult by the smaller size of the unit cell and correspondingly of the ligaments on which strain gages needed to be applied.

Similarly to configurations *a* and *b*, the numerical model for configuration *c* is able to capture the trailing edge displacement variation for increasing applied loads (Figure 18). As in the case of configuration *b*, no residual displacements are observed. Variations of strain at selected locations do not show as good of an agreement as in the previous two cases, but clearly confirm the absence of nonlinear trends in the curve, and of residual strains upon unloading (Figure 19). The lack of agreement on strains in

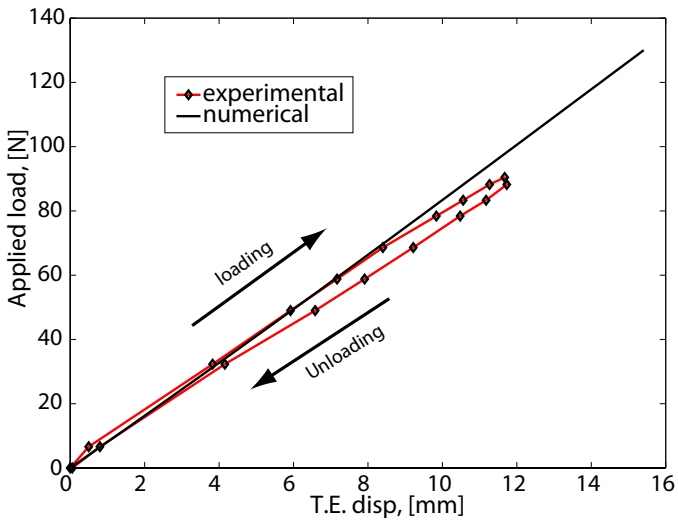

Figure 18. Numerical and experimental trailing-edge displacement for configuration *c*.

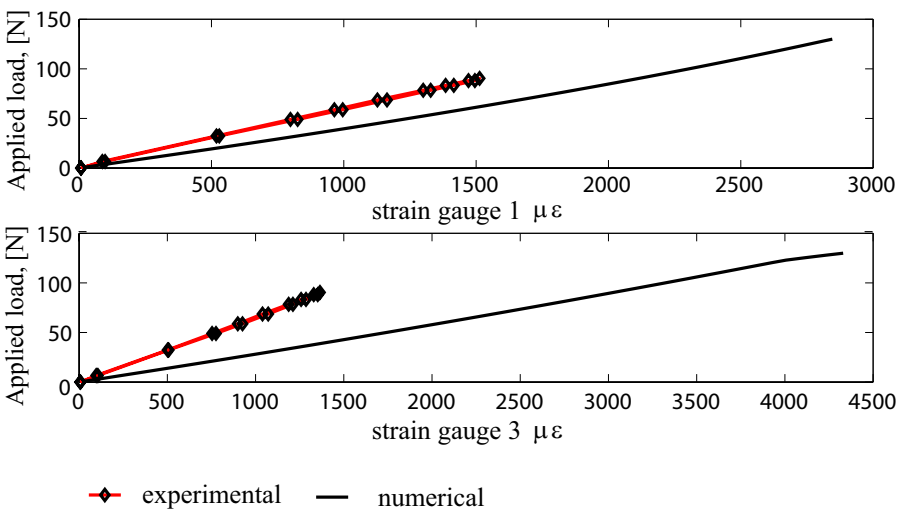

Figure 19. Numerical and experimental strain for configuration *c*.

this and in the previous two cases may indicate shortcomings in the FE model, and a lack in accuracy in the strain gage positioning. It is interesting to note, however, that the numerical model is able to accurately reproduce the displacement/load variation and to show the linear relationships in all three cases. In addition, the experimental results confirm the strong dependence of the airfoil compliance on the core configuration as demonstrated by the direct comparison of trailing edge displacement versus load, experimental and numerical, for the three configurations, which is presented in Figure 20.

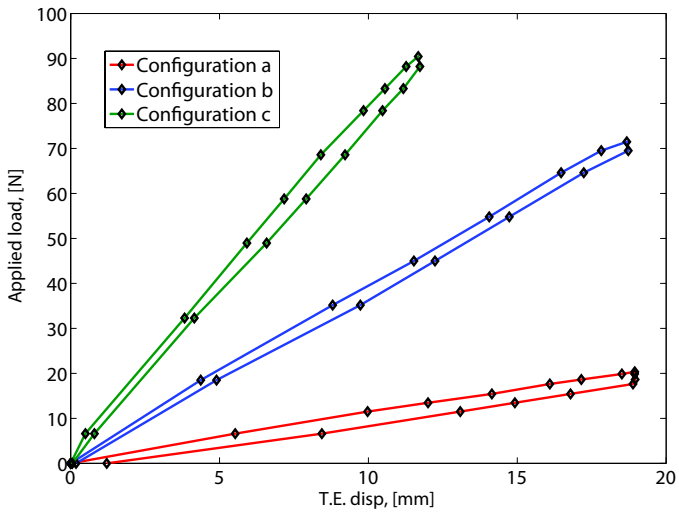

Figure 20. Comparison of trailing-edge displacement for the three considered configurations.

5. Conclusions

This paper presents numerical and experimental investigations performed on a novel airfoil configuration. In the proposed design, a chiral cellular structure is accommodated within the airfoil profile to provide it with chordwise bending compliance, combined with the ability of carrying torsional loads. The compliance characteristics of airfoils with different core designs are investigated with the objective of assessing the ability of the structure to undergo large deflections while remaining in the linear range of the material, and the strong influence of the core design on the overall performance of the airfoil. To this end, three configurations have been designed, manufactured and tested. The tests are guided by numerical investigations performed using nonlinear FE models. A comparison of numerical and experimental results shows that the devised numerical models are overall capable of providing estimates of the onset of plastic deformations and can predict the trailing-edge displacement resulting from assigned loads. Numerical and experimental results also show the ability of the considered airfoil design to undergo significant camber changes. The same analyses suggest the opportunity of achieving significant performance variations through the proper selection of a limited number of parameters which define the core geometry. A natural application for this concept is aeroelastic tailoring. Future investigations will therefore address the performance of three dimensional wings with chiral ribs, or of wings with an internal, three dimensional network which extends the configuration herein investigated. Dynamic characterization of the proposed truss core airfoil should also be performed.

References

[ANSYS 2005] P. Kohnke (editor), *ANSYS theory reference*, Release 10.0 ed., Canonsburg, PA: ANSYS, 2005, Available at http://www.we.mtu.edu/users/applist/appdocs/ansys/ansys_theory_ref.pdf.

[Bae et al. 2004] J. S. Bae, T. M. Seigler, D. J. Inman, and I. Lee, "Aerodynamic and aeroelastic considerations of a variable-span morphing wing", pp. 2378–2396 in *45th AIAA/ASME/ASCE/AHS/ASC Structures, Structural Dynamics and Materials*

Conference (Palm Springs, CA, 2004), AIAA, Reston, VA, 2004, Available at http://www.aiaa.org/content.cfm?pageid=2. Paper #2004-1726.

[Bornengo et al. 2005] D. Bornengo, F. Scarpa, and C. Remillat, "Evaluation of hexagonal chiral structure for morphing airfoil concept", *Proc. Inst. Mech. Eng. G, J. Aerosp. Eng.* **219**:3 (2005), 185–192.

[Büter et al. 2001] A. Büter, U. C. Ehlert, D. Sachau, and E. Breitbach, "Adaptive rotor blade concepts: direct twist and camber variation", pp. 1–12 (Section 19) in *Active control technology for enhanced performance operational capabilities of military aircraft, land vehicles and sea vehicles* (Braunschweig, 2000), RTO Meeting Proceedings **51**, NATO Research and Technology Organization, Neuilly-sur-Seine, 2001, Available at ftp://ftp.rta.nato.int//PubFullText/RTO/MP/RTO-MP-051/MP-051-MSSM-19.PDF. Report RTO-MP-051.

[Cadogan et al. 2004] D. Cadogan, T. Smith, F. Uhelsky, and M. MacCusick, "Morphing airfoil wing development for compact package unmanned aerial vehicles", pp. 3205–3217 in *45th AIAA/ASME/ASCE/AHS/ASC Structures, Structural Dynamics and Materials Conference* (Palm Springs, CA, 2004), AIAA, Reston, VA, 2004, Available at http://www.aiaa.org/content.cfm?pageid=2. Paper #2004-1807.

[Campanile and Sachau 2000] L. F. Campanile and D. Sachau, "The belt-rib concept: a structronic approach to variable camber", *J. Intell. Mater. Syst. Struct.* **11**:3 (2000), 215–224.

[Culik 2003] F. E. C. Culik, "The Wright brothers: first aeronautical engineers and test pilots", *AIAA J.* **41**:6 (2003), 985–1006.

[Ghiringhelli and Mantegazza 1994] G. Ghiringhelli and P. Mantegazza, "Linear, straight and untwisted anisotropic beam section properties from solid finite elements", *Compos. Eng.* **4**:12 (1994), 1225–1239.

[Herbert et al. 2006] E. G. Herbert, W. C. Oliver, and G. M. Pharr, "On the measurement of yield strength by spherical indentation", *Philos. Mag.* **86**:33 (2006), 5521–5539.

[Hodges and Pierce 2002] D. Hodges and G. Pierce, *Introduction to structural dynamics and aeroelasticity*, Cambridge Aerospace Series **15**, Cambridge University Press, New York, 2002.

[Kudva 2004] J. N. Kudva, "Overview of the DARPA smart wing project", *J. Intell. Mater. Syst. Struct.* **15**:4 (2004), 261–267.

[Lakes 1991] R. S. Lakes, "Deformation mechanisms in negative Poisson's ratio materials: structural aspects", *J. Mater. Sci.* **26**:9 (1991), 2287–2292.

[McGowan et al. 2003] A. R. McGowan, D. E. Cox, B. S. Lazos, M. R. Waszak, D. L. Raney, E. J. Siochi, and P. S. Pao, "Biologically inspired technologies in NASA's morphing project", pp. 1–13 in *Smart structures and materials 2003: electroactive polymer actuators and devices (EAPAD)* (San Diego, 2003), edited by Y. Bar-Cohen, Proceedings of SPIE **5051**, SPIE, Bellingham, WA, 2003.

[Monner et al. 2000] H. P. Monner, D. Sachau, and E. Breitbach, "Design aspects of the elastic trailing edge for an adaptive wing", pp. 1–8 (Section 14) in *Structural aspects of flexible aircraft control* (Ottawa, 1999), RTO Meeting Proceedings **36**, NATO Research and Technology Organization, Neuilly-sur-Seine, 2000, Available at ftp://ftp.rta.nato.int//PubFulltext/RTO/MP/RTO-MP-036/MP-036-14.pdf. Report RTO-MP-036.

[Prall and Lakes 1997] D. Prall and R. S. Lakes, "Properties of a chiral honeycomb with a Poisson's ratio of -1", *Int. J. Mech. Sci.* **39**:3 (1997), 305–314.

[Spadoni and Ruzzene 2006] A. Spadoni and M. Ruzzene, "Static aeroelastic behavior of chiral-core airfoils", *J. Intell. Mater. Syst. Struct.* (2006). In press.

[Spadoni et al. 2006] A. Spadoni, M. Ruzzene, and F. Scarpa, "Dynamic response of chiral truss-core assemblies", *J. Intell. Mater. Syst. Struct.* **17**:11 (2006), 941–952.

[Trenker 2003] M. Trenker, "Design concepts for adaptive airfoils with dynamic transonic flow control", *J. Aircr.* **40**:4 (2003), 734–740.

Received 30 Nov 2006. Accepted 25 Mar 2007.

ALESSANDRO SPADONI: alessandro@gatech.edu
School of Aerospace Engineering, Georgia Institute of Technology, 270 Ferst Drive, Atlanta, GA, United States

MASSIMO RUZZENE: Massimo.ruzzene@ae.gatech.edu
School of Aerospace Engineering, Georgia Institute of Technology, 270 Ferst Drive, Atlanta, GA, United States